Geomechanics and Engineering, *Vol. 33, No. 1 (2023) 101-112*
https://doi.org/10.12989/gae.2023.33.1.101

Dynamic behavior of submerged floating tunnels at the shore connection considering the use of flexible joints

Seok-Jun Kang[1a], Minhyeong Lee[2b], Jun-Beom An[1c], Dong-Hyuk Lee[1d] and Gye-Chun Cho*[1]

[1]*Department of Civil and Environmental Engineering, Korea Institute of Science and Technology, 291 Daehak-ro, Yuseong-gu, Daejeon 305-701, Republic of Korea*
[2]*Disposal Performance Demonstration Research Division, Korea Atomic Energy Research Institute, 111 Daedeok-daero 989Beon-gil, Yuseong-gu, Daejeon, Republic of Korea*

(*Received October 27, 2022, Revised March 13, 2023, Accepted March 15, 2023*)

Abstract. When a submerged floating tunnel is connected to the ground, there is a risk of stress concentration at the shore connection owing to the displacement imbalance caused by low confinement pressures in water and high confinement pressures in the ground. Here, the effects of the boundary condition and stiffness of the joints installed at the shore connection on the behaviors of a submerged floating tunnel and its shore connection were analyzed using a numerical method. The analysis results obtained with fixed and ground boundaries were similar due to the high stiffness of the ground boundary. However, the stability of the shore connection was found to be improved with the ground boundary as a small displacement was allowed at the boundary. The effect of the joint stiffness was evaluated by investigating the dynamic behavior of the submerged floating tunnel, the magnitude of the load acting on the bored tunnel, and the stress distribution at the shore connection. A lower joint stiffness was found to correspond to more effective relief of the stress concentration at the shore connection. However, it was confirmed that joints with low stiffness also increase the submerged floating tunnel displacement and decrease the frequency of the dynamic behavior, causing a risk of increased resonance when wave loads with low frequency are applied. Therefore, it is necessary to derive the optimal joint stiffness that can achieve both stress concentration relief and resonance prevention during the design of shore connections to secure their dynamic stability.

Keywords: ground boundary; flexible joint; numerical method; shore connection; submerged floating tunnel

1. Introduction

To cross the sea, it is necessary to use a special means of transportation or utilize a route connecting continents. Representative methods providing a pathway above sea level include transportation means such as airplanes, ships, and bridges. However, these methods have limitations in that they are significantly affected by weather conditions or the distance between continents. As an alternative, subsea tunnels that are constructed under the seabed or immerged tunnels that are placed on the seabed have been proposed and are being used in various areas. However, the possibility and economic feasibility of constructing these types of tunnels are greatly affected by the depth of the seabed. If the seabed is deep, a subsea tunnel must be constructed in a long section from the surface to a deep depth. Additionally, if the seabed is deep, it is difficult to place an immersed tunnel at the targeted seabed. These types of tunnels exhibit limitations in terms of their construction in the deep seabed, which is accompanied by increases in construction cost and time (Jiang *et al.* 2018). As an alternative, submerged floating tunnels (SFTs) have been proposed (Grant 1986). SFTs are floated at a specific water level using methods such as pontoons and tethers (Won and Kim 2018). They are less affected by the weather above the water surface or by waves and are comparatively free from the influence of ground motion (Martire 2010). SFTs dynamically move during operation owing to tidal and wave loads (Long *et al.* 2009), and therefore, their dynamic behavior must be precisely analyzed. To provide a path between lands through water, SFTs must be connected to the ground (Xiao and Huang 2010). Because SFTs are connected to the ground, the tunnels of these systems are distinguished as bored tunnels in the ground and SFTs in water. These tunnels exhibit different constraint conditions, and the risk of stress concentration at the shore connection point is an essential issue in SFT design (Kang *et al.* 2020).

Previous studies related to SFT design in a specific area (Mazzolani *et al.* 2007; Martinelli *et al.* 2010; Mazzolani *et al.* 2010; NPRA 2016) have mainly focused on the hydrodynamic behavior of SFTs. The method to stabilize the SFTs while floating in water (e.g., mooring and tethering methods) at a specific depth (Jakobsen 2010) and the dynamic stability according to the mooring method that is used have been evaluated (Jin *et al.* 2020). To design an SFT with adequate dynamic stability, the structural characteristics (Youshi and Fei 2010), dynamic load characteristics (Cifuentes *et al.* 2015), and buoyancy-to-

*Corresponding author, Professor
E-mail: gyechun@kaist.edu
[a]Postdoctoral Researcher
[b]Postdoctoral Researcher
[c]Ph.D. Candidate
[d]Postdoctoral Researcher

ISSN: 2005-307X (Print), 2092-6219 (Online)

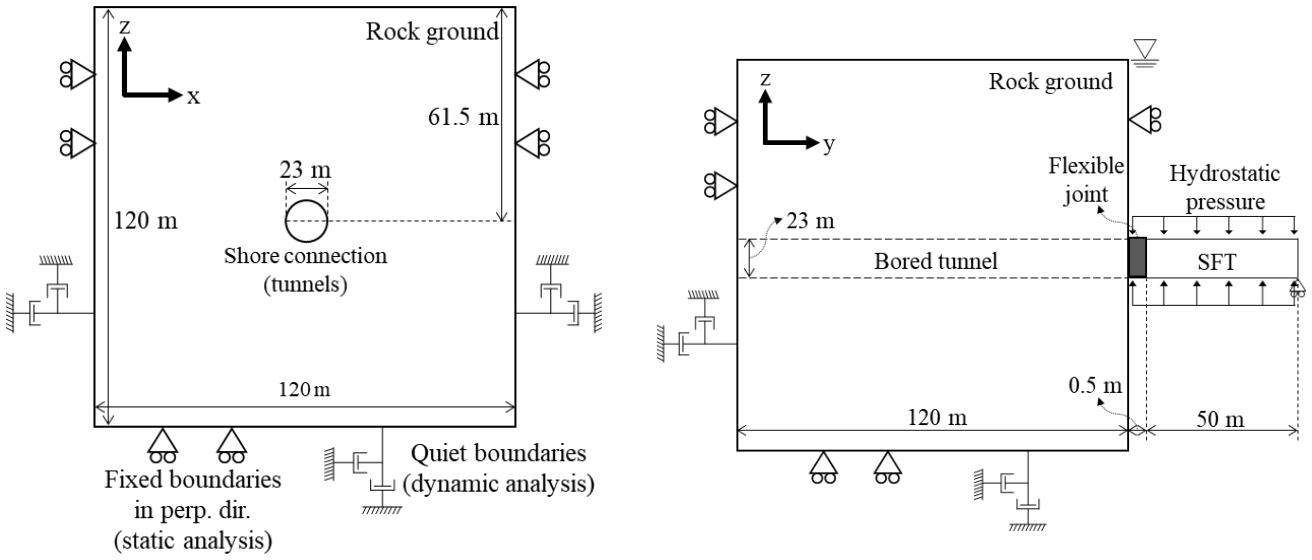

Fig. 1 Numerical model for the shore connection of SFT displayed in (a) front view and (b) side view

weight ratio (Jin and Kim 2017) have been considered as important design parameters. Additionally, Jin and Kim (2021) conducted a numerical analysis to evaluate the effects of key design parameters on the dynamic behavior of SFTs. However, these studies did not consider shore connections. As such, no appropriate suggestions for shore connection point designs in which an SFT is connected to the ground have yet been made.

Xiao and Huang (2010) conducted a numerical study simulating earthquake excitation on an SFT considering a shore connection design. However, their study considered the shore connection as a bearing element at the boundary without simulating the ground or bored tunnels. Park *et al.* (2022) conducted a series of parametric studies to evaluate the effects of shore connection design with a ring-type joint on the dynamic characteristics of the SFT. They found that the joint between the SFT and boundary can control the resonance frequency of the entire SFT system. Kang *et al.* (2020) conducted a numerical analysis to evaluate the stress concentrations at shore connections under static conditions. They found that a shore connection with a flexible joint could alleviate the stress concentration at this juncture. In addition, their study suggested that the use of a grouting material with low stiffness can absorb the displacement transferred from the SFT, causing the stress to be distributed into the grouted layer rather than concentrated at the shore connection. This study showed that allowing displacement at the boundary between the bored tunnel and SFT may provide a stable design; however, consideration of the dynamic behavior was not included.

Therefore, the current study aims to conduct a three-dimensional numerical analysis to evaluate the effect of shore connection design under dynamic loading conditions. When a dynamic load is applied to the SFT, the stress and strain occurring at the shore connection are observed. The shore connection design is a ring-type joint located between the SFT and bored tunnel. To overcome the limitations of previous studies in which the boundary of the SFTs was assumed to be fixed, the ground and bored tunnels are simulated such that they are connected to the SFT at the shore connection point. Numerical simulations representing both the fixed and ground boundary conditions are conducted, and the results are compared. Additionally, shore connection designs using various ring joint stiffnesses are simulated to evaluate their effects on the dynamic behavior of the SFT. The stress distributions and displacements in SFTs with various shore connection designs are analyzed to understand the effect of ring joint stiffness on the stability of shore connections under static and dynamic conditions.

2. Numerical methodology

2.1 Introduction

The SFT, its shore connection, bored tunnel, and ground surrounding the bored tunnel were simulated using a three-dimensional numerical model that included several assumptions to simplify the situation. The numerical model was created using the commercial software Fast Lagrangian Analysis of Continua in 3-Dimensions (FLAC 3D) ver. 5.0 (Itasca Consulting Group, Inc.) based on the finite difference method.

The connection between SFT modules (i.e., the fixed part of mooring lines) shows little displacement and acts as the boundary condition, causing differences in behavior between SFT modules at both sides (Jin and Kim 2017). Therefore, among all SFT modules, one module closest to the shore is expected to have a dominant influence on the shore connection behavior. In this study, only one SFT module connected to the shore connection was formed to simplify the numerical simulation. This single SFT module has a length equal to the distance between the mooring lines and serves to transfer the dynamic load generated over the

Table 1 Properties of the ground

Type	Value
Rock type	Granite
Constitutive model	Mohr-Coulomb
Density [kg/m^3]	2700
Elastic modulus [GPa]	40
Shear modulus [GPa]	16
Bulk modulus [GPa]	26.7
Friction angle [°]	30
Cohesion [MPa]	10
Tensile strength [MPa]	16

Table 2 Properties of the tunnels

Type	Value
Tunnel material	Concrete
Constitutive model	Linear elastic
Tunnel diameter [m]	23
Elastic modulus [GPa]	30
Material density [kg/m^3]	3000
Segment thickness [m]	1.0
Segment length [m]	50

entire length of the SFT to the ground through the shore connection. The characteristics of the dynamic load were determined based on the results reported by Jin and Kim (2017), who numerically studied the hydrodynamic behavior of an entire SFT. The numerical model was designed such that a dynamic load was applied to one end of the SFT module and transmitted to the shore connection point at the opposite end. The purpose of this study was to analyze the change in the behavior of the ground and tunnels around the shore connection according to the shore connection conditions. The shore connection conditions to be evaluated were set as the boundary conditions (i.e., fixed boundary and ground boundary) along with the joint type used between tunnels.

2.2 Numerical model

2.2.1 Numerical model formation

The numerical model simulated a single module SFT, shore connection, bored tunnel, and ground (Fig. 1). The maximum mesh size was set as 1.0 m, which is sufficiently short for the dynamic load to be properly reflected in the numerical model (Kuhlemeyer and Lysmer 1973). The ground was formed using the Mohr-Coulomb model to simulate the elastoplastic behavior of homogenous granite. The tunnels and joints between the tunnels were formed using a linear elastic model. The properties of each element were assumed to be general material characteristics, as shown in Tables 1 and 2. A ring joint with a length of 0.5 m was simulated between the SFT and bored tunnel at the shore connection as a design parameter. The interfaces between the ring joint and SFT and between the ring joint and bored tunnel were constituted with a rigid connection.

The boundaries of the ground were formed by fixation at a sufficient distance from the shore connection to avoid affecting the SFT behavior during static analysis. During the dynamic analysis, the boundaries were adjusted to be quiet-type boundaries to allow the correct reaction forces at the boundary (Itasca 2013). The boundary conditions at the ends of a single SFT module were determined according to assumptions related to the simplified situation using a single module. One boundary of the SFT module (the left end of the SFT module in Fig. 1) was fixed in the vertical and longitudinal directions. Another boundary (the right end of the SFT module in Fig. 1) indicates the shore connection; therefore, this boundary condition is determined considering the ground surrounding the shore connection and ring joint. The boundary at the shore connection was simulated for two cases: a fixed boundary and a ground boundary. The fixed boundary condition represented the same situation as that considered in previous studies that did not consider the ground at the end of the SFT. The numerical model representing the ground was fixed when simulating the fixed boundary condition. However, the ground boundary condition was formed using a shore connection, which included the bored tunnel and surrounding ground. This condition allows ground behavior to affect the dynamic SFT motion.

2.2.2 Assumptions for environmental conditions

Submarine environmental condition

The SFT and its shore connection are affected by both marine and geotechnical environments. To consider the marine environment, the hydrostatic pressure acting on the surface of the SFT, buoyancy acting on the SFT body, and dynamic force acting on the end of the SFT were simulated. The pressures were derived by assuming that the SFT was placed at a depth of 61.5 m, buoyancy-weight ratio of 1.38, and hydrostatic pressure of 620 kPa, based on a previous study (Jin and Kim 2017). The dynamic load applied at the end of the SFT, which represents the wave loads acting on the entire SFT, was assumed to be a sinusoidal wave with an amplitude of 26 MN and loading frequency of 2 Hz.

Ground environmental condition

To consider geotechnical environmental conditions, the soil-tunnel interaction for the bored tunnel and ground nonlinearity were simulated. The soil-tunnel interaction was applied based on the interface properties, wherein the coupling stiffness, $k_{coupling}$, is defined as

$$k_{coupling} = \max\left[\frac{K+\frac{4}{3}G}{\Delta z_{min}}\right], \quad (1)$$

where K is the bulk modulus, G is the shear modulus, and Δz_{min} is the smallest dimension of the adjoining zone at the interface (Itasca 2013).

The ground nonlinearity was considered using hysteretic damping. The damping characteristics were input into the numerical model using the Hardin model (Hardin and Drnevich 1972) with the reference strain adjusted to 0.06, which is a representative value for rock ground (Seed *et al.* 1986).

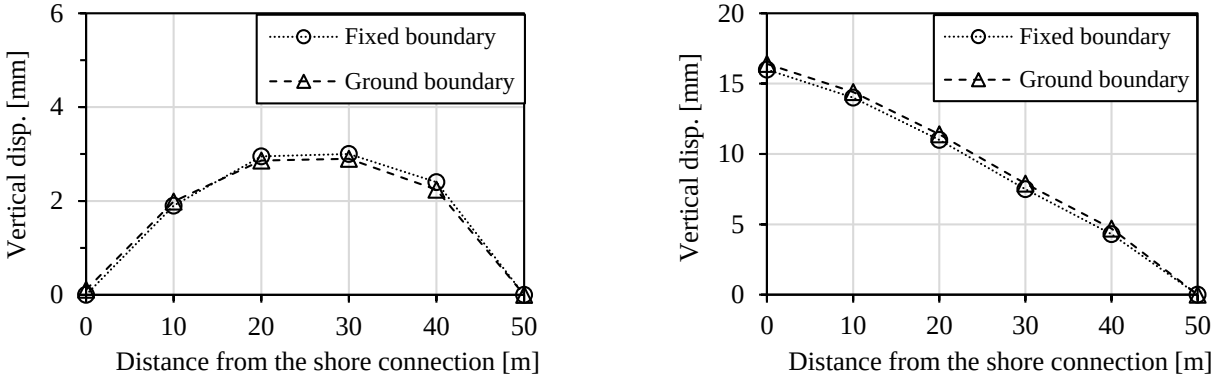

Fig. 2 Displacement of the SFT with a ring joint composed of (a) concrete and (b) reinforced rubber according to the boundary type under static loading conditions

Table 3 Numerical cases

Shore connection	Elastic stiffness	Poisson's ratio
Concrete	30.0 GPa	0.15
Reinforced rubber	12.75 MPa	0.45
Rubber 1	8.5 MPa	0.45
Rubber 2	4.25 MPa	0.45
Rubber 3	2.13 MPa	0.45
Rubber 4	1.06 MPa	0.45

2.3 Numerical analysis procedure

2.3.1 Simulation steps

Several preparatory steps were taken to create a proper stress state before conducting the main analysis to improve the validity of the numerical analysis. First, a static analysis was performed to simulate the stress conditions under gravitational and hydrostatic conditions by simulating only the ground before tunnel construction. Subsequently, numerical models for the underground bored tunnel and SFT were constructed. Environmental factors other than dynamic loads were considered through a static analysis that reflected the tunnel's weight, water pressure acting on the tunnel, and buoyancy. Finally, the behaviors of the tunnel and ground were evaluated by applying a dynamic load to the statically equilibrated model.

2.3.2 Simulation cases

To evaluate the effects of the boundary condition and ring joint stiffness, each parameter was varied in the numerical simulation cases. The boundary conditions were determined as fixed and ground boundary conditions. To simulate the fixed boundary condition, global fixation was applied to all nodes of the mesh corresponding to the ground. The ground boundary was simulated by connecting the SFT to the ground using a ring joint. In addition, the material of the ring joint was considered as a variable in the numerical analysis. A typical tunnel-to-tunnel joint was used to continuously connect the tunnel lining made of concrete, without including a separate connecting body. In this study, the effect of the joint on the dynamic behavior of the overall SFT was investigated simulating the typical case (i.e., a concrete connection), as well as five other cases where the joint was made of reinforced rubber. The properties of the joints for each case are summarized in Table 3. In each case, all conditions other than the joint properties were identical.

3. Behaviors at the shore connection according to the boundary condition

Fixed and ground boundary conditions were simulated using the numerical model. The behaviors of the SFT and ring joint located between the SFT and boundary were analyzed according to the boundary conditions. In addition, the ring joint was simulated using concrete and reinforced rubber at the shore connection points with identical SFT properties, and the effect of the ring joint type was also examined.

3.1 Static conditions with a buoyant SFT

Before the dynamic load was applied, the SFT module received a vertical upward load via a buoyancy force that was greater than the gravitational force. In the static equilibrium state, reaction forces occur at the boundaries of both ends (i.e., the mooring line at one end and the shore ground at the other end) that act against the buoyancy of the SFT module. The SFT exhibits bending deformation between the two fixed boundaries, as shown in Fig. 2, according to the boundary condition at the shore connection. The two cases with fixed and ground boundary conditions showed similar SFT displacements. However, the type of ring joint significantly affected the SFT displacement. When simulating a rigid connection by constructing a ring joint with concrete (Fig. 2(a)), the largest vertical displacement occurred at the center of the SFT, and the largest displacement occurred at the shore connection when using a flexible material for the ring joint (Fig. 2(b)).

Figs. 3 and 4 show the principal stress distributions occurring in the SFT at a section of the fixed part near the

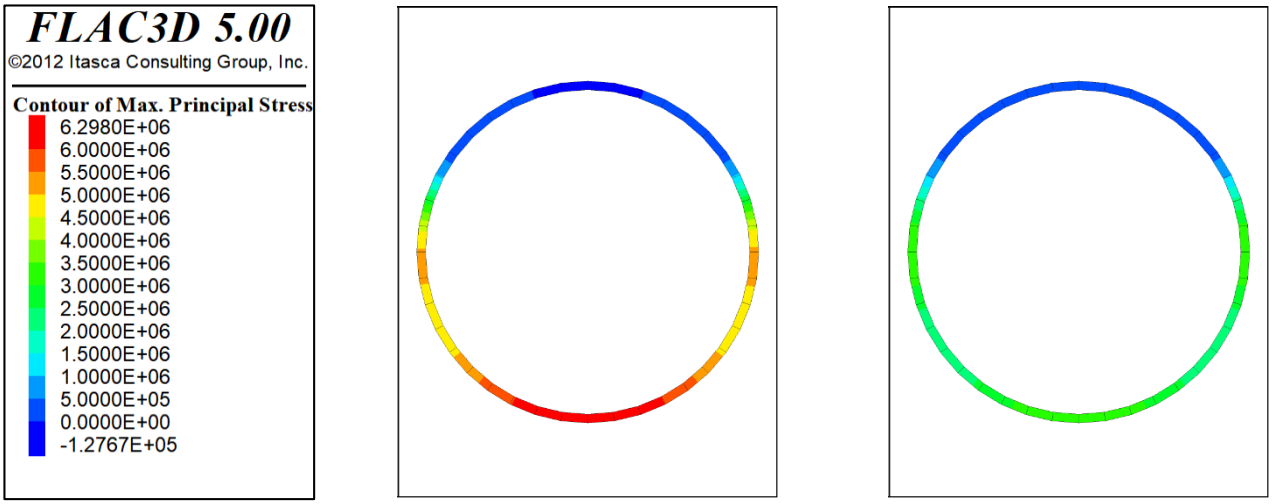

Fig. 3 Principal stress distributions in an SFT with a joint composed of (a) concrete and (b) reinforced rubber connected to a fixed boundary under static loading conditions

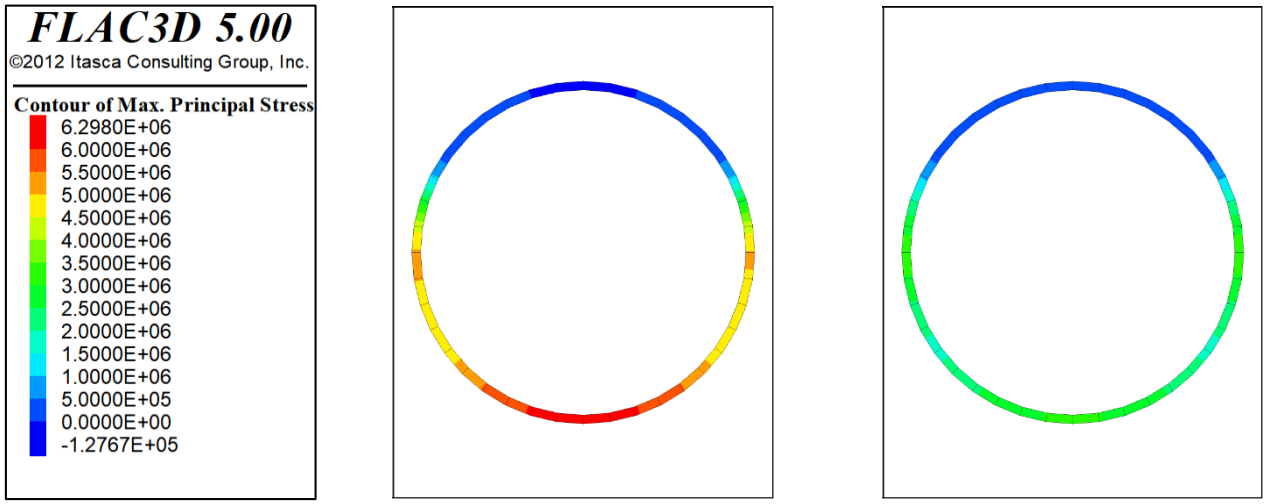

Fig. 4 Principal stress distributions in an SFT with a joint composed of (a) concrete and (b) reinforced rubber connected to a ground boundary under static loading conditions

mooring line when the shore connection was simulated as a fixed boundary. Compared with the case in which a stiff ring joint was used, the magnitude of the stress was significantly reduced when a flexible joint was used. When assuming a fixed boundary without ground deformation (Fig. 3), a larger stress occurred compared to the case in which ground deformation was allowed (Fig. 4), but the effect of the joint-type was dominant.

In the cases where the ground was simulated, the displacement of the ground according to the type of ring joint that was used is shown in Fig. 5. In the case of a stiffer joint, the buoyancy force of the SFT is transmitted to the ground, causing stress concentration near the shore connection. However, when using a flexible joint, a very small amount of displacement occurred by lowering the magnitude of the stress applied to the ground because of the larger deformation of the joint. These static analysis resultsare consistent with the stress concentration pattern of the shore connection and the effect of the flexible joint reported by Kang *et al.* (2020).

3.2 Dynamic condition

The SFT dynamic behavior in the presence of a lateral dynamic load according to boundary condition and joint type was analyzed in terms of the maximum displacement and frequency of the SFT. The fixed and ground boundaries showed similar effects on the SFT behavior because a relatively small dynamic load was applied in this study, causing a small ground strain at the boundary. However, the SFT behavior was significantly affected by a change in joint type (Fig. 8). When a flexible joint was used, a maximum displacement of approximately 70 cm and a frequency of 1.86 were observed, but when a stiff joint was used, a

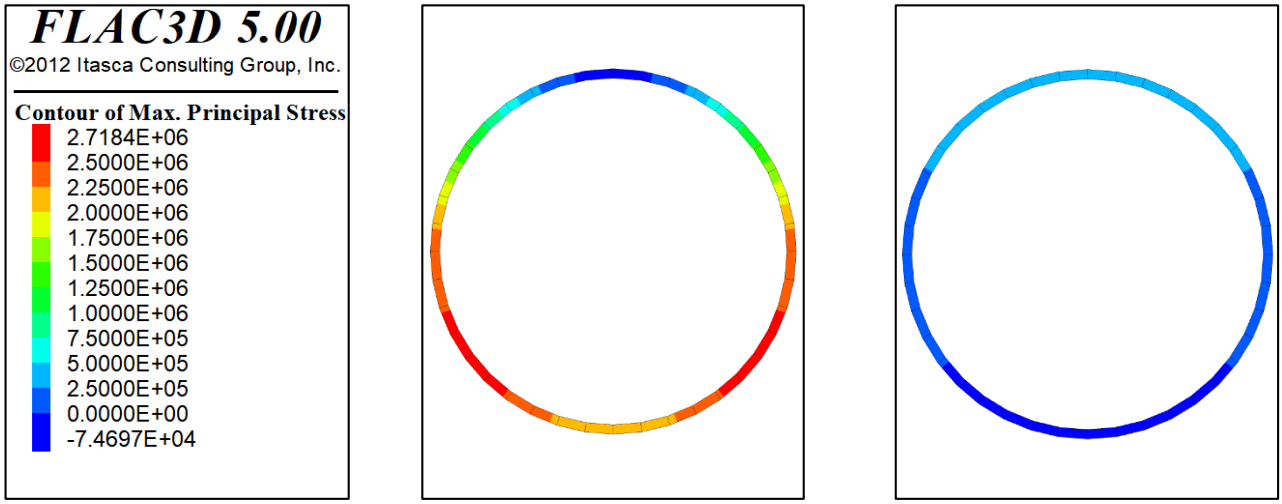

(a) (b)

Fig. 5 Principal stress distributions in a joint composed of (a) concrete and (b) reinforced rubber connected to a fixed boundary under static loading conditions

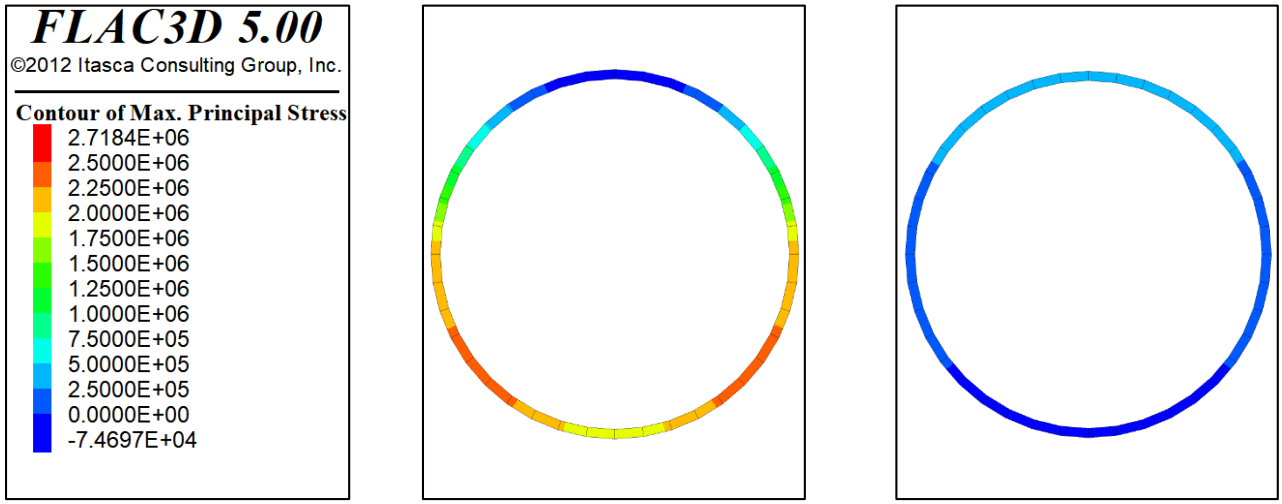

(a) (b)

Fig. 6 Principal stress distributions in a joint composed of (a) concrete and (b) reinforced rubber connected to a ground boundary under static loading conditions

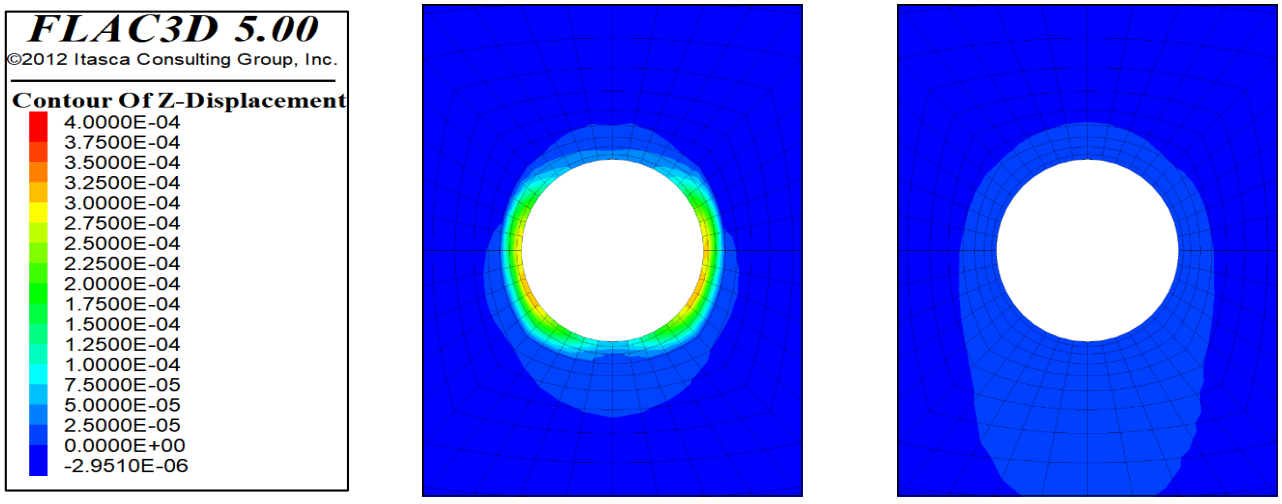

(a) (b)

Fig. 7 Vertical displacement distributions in the ground at the shore connection point when a joint composed of (a) concrete and (b) reinforced rubber was connected to a ground boundary under static loading conditions

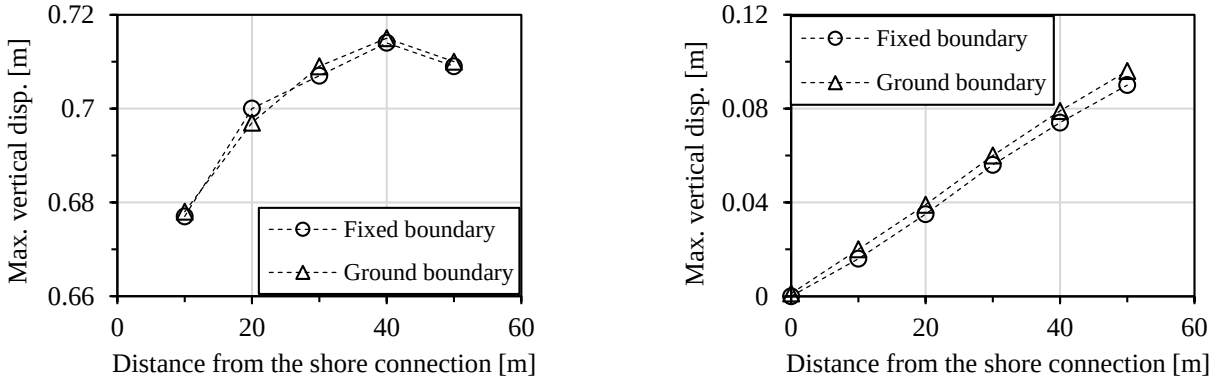

Fig. 8 Maximum vertical displacements of the SFT with a joint composed of (a) concrete and (b) reinforced rubber connected to fixed and ground boundaries under dynamic loading conditions

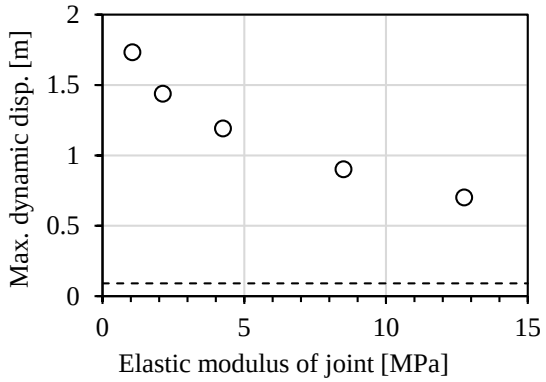

Fig. 9 Maximum displacement of one end of the SFT according to the joint stiffness

maximum displacement of approximately 10 cm and a frequency of 6.125 were observed. These results are consistent with those reported by Park *et al.* (2022), in which the level of displacement decreased and the resonance frequency increased as the stiffness of the joint connecting the boundary and SFT increased.

4. Effect of the stiffness of the flexible joint

To understand the effect of varied joint stiffness on the behavior of the SFT at the shore connection, the results of numerical simulations using joints with various properties (Table 3) were compared. The dynamic movement of the SFT and resulting stress distribution at the ground connection were observed.

4.1 Static condition with a buoyant SFT

The effect of varying the flexible joint stiffness was evaluated by measuring the displacement of the SFT in a static equilibrium state before dynamic load application. As the stiffness was varied, it was confirmed that the bending behavior of the SFT occurred in a manner similar to that shown in Fig. 2. When a joint with high stiffness was used, the maximum displacement occurred near the center of the SFT, as shown in Fig. 2(a). However, when a joint with low stiffness was used, the location where the maximum displacement occurred changed so that it was near the shore connection. As the joint stiffness decreased, the maximum displacement in the shore connection increased. As the SFT floats upward because of buoyancy, stress occurs at the shore connection, which is constrained by the shore connection point. A stiffer connection caused greater stress at the bottom of the SFT. When a joint with low stiffness was installed, the stress caused by SFT displacement was not concentrated at the shore connection and was transferred to the surrounding ground or bored tunnel. This result is remarkably similar to that obtained in a previous study (Kang *et al.* 2020).

4.2 Dynamic condition

A dynamic analysis was conducted after the static analysis, which included the statically equilibrated stress state, by additionally applying a dynamic load at the end of the SFT in the lateral direction. To investigate only the dynamic analysis results, the displacement that occurred during the static analysis was initialized as zero, and the dynamic load was applied in the lateral direction. The dynamic load was applied for 5 s, and the analysis results were evaluated based on the peak point of the last loading cycle. The SFT, bored tunnel, shore connection, and surrounding ground were observed in terms of the distribution of strain or stress.

4.2.1 Submerged floating tunnel behavior

The SFT is restrained by hydrostatic pressure, which is much smaller than the earth pressure that confines the shore connection. Because the SFT is composed of a perfectly elastic body, dynamic behavior similar to the input dynamic load in the form of a harmonic wave was observed. Because a dynamic load was applied at the end of the SFT, the displacement observed at the end was the largest. The displacement decreased as the shore connection was approached. When a flexible joint was used, the displacement of the SFT near the shore connection increased, as shown in Fig. 9. Compared with the use of a

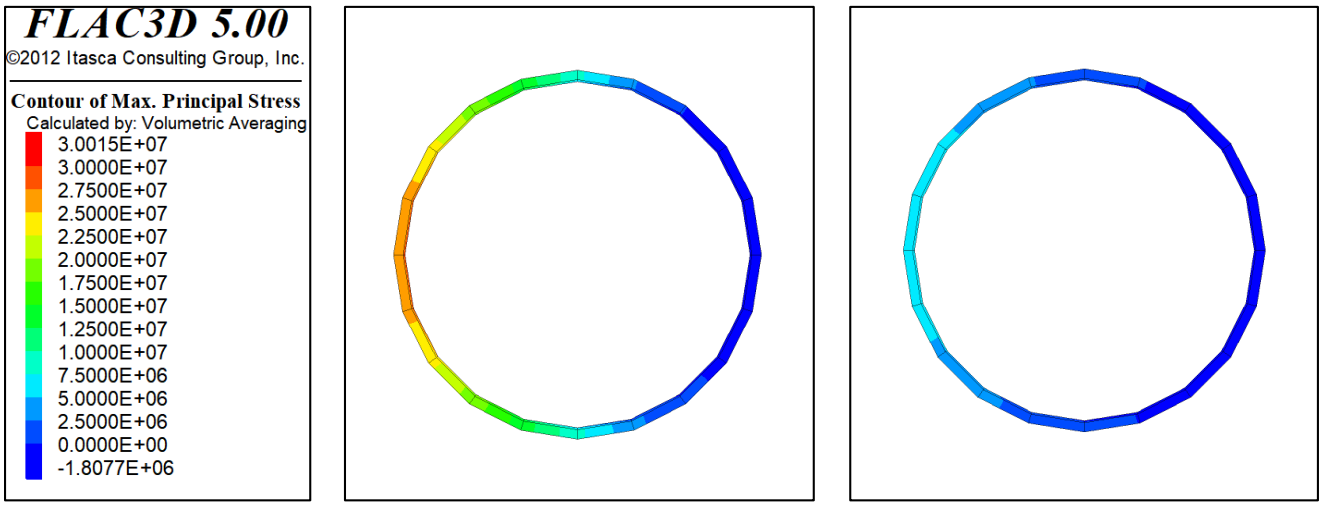

(a) (b)

Fig. 10 Principle stress distributions in the shore connection composed of (a) concrete and (b) rubber as the result of dynamic analysis

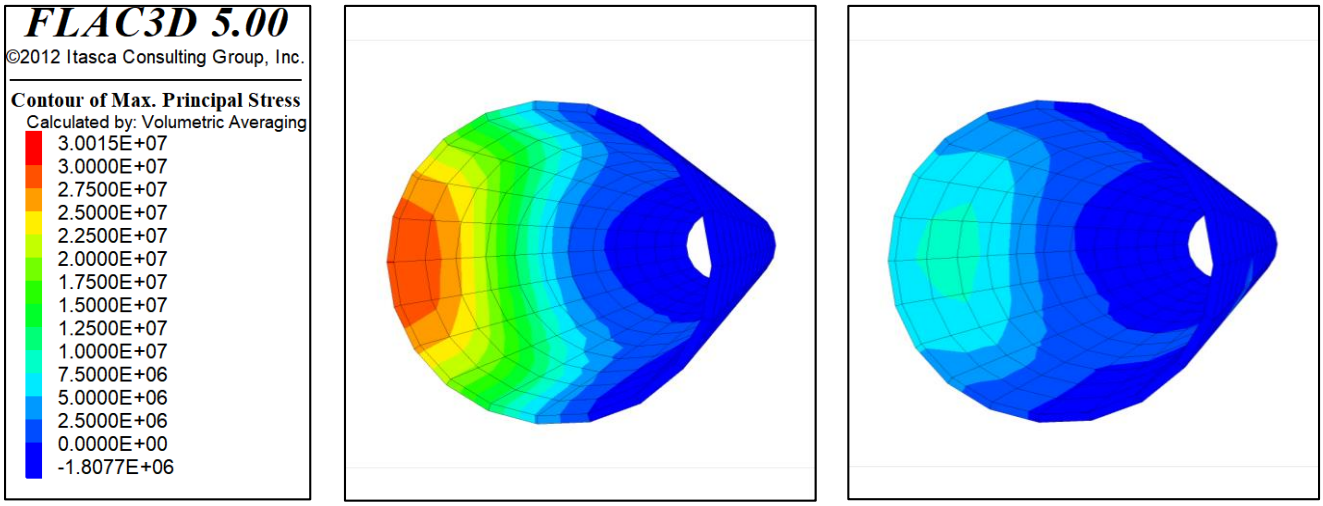

(a) (b)

Fig. 11 Principal stress distributions in the bored tunnel with a joint composed of (a) concrete and (b) rubber

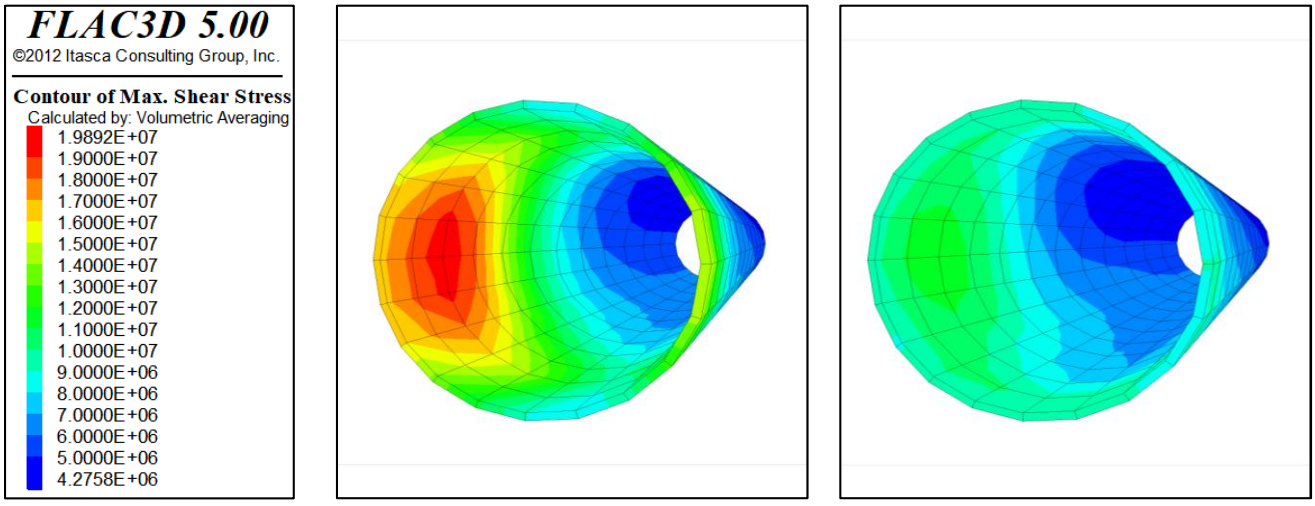

(a) (b)

Fig. 12 Shear stress distributions in the bored tunnel with a joint composed of (a) concrete and (b) rubber

concrete joint (dotted line), the maximum displacement was seven times larger when a soft rubber joint was used. This result implies that the maximum displacement is dominantly controlled by the joint stiffness, which can be considered as a boundary condition. Therefore, the design of the shore connection Generally, the resonant frequency of an SFT is much larger must include considerations related to resonance. As the joint becomes stiffer, the resonant frequency of the SFT increases (Park *et al.* 2022). than the loading frequency of tidal or current loads. However, if the resonant frequency decreases with a flexible joint, the increased displacement of the SFT can increase the risk of excessive displacement with resonance.

4.2.2 Ring joint behavior

As a lateral cyclic load was applied, the shore connection exhibited stress concentrations according to the lateral displacement of the SFT (Fig. 10). As the shore connection was made of a soft material, the displacement of the overall shore connection and SFT increased. However, the magnitude of the distributed stress decreased, and the stress concentration was alleviated. This tendency is similar to that observed in the static analysis. However, because the resonance and displacement levels are of great importance under dynamic conditions, the optimal shore connection stiffness must be determined considering the dynamic characteristics of the entire system, including the ground, shore connection, and SFT. Considering only the shore connection, if it is made of a soft material, the SFT stress is reduced while the displacement is significantly increased. Therefore, the stiffness of the material should be sufficiently high and satisfy the allowable SFT displacement.

4.2.3 Underground bored tunnel behavior

The dynamic load caused by the SFT behavior was transmitted to the bored tunnel via the shore connection. Therefore, the joint stiffness affects the characteristics of the load transferred to the bored tunnel. As shown in the results of the principle (Fig. 11) and shear (Fig. 12) stress distributions in the bored tunnel, the magnitude of the stress was not large considering the general expected strength of the concrete tunnel. However, it is necessary to evaluate the stress distribution characteristics in the bored tunnel according to the shore connection design to prepare for situations in which a large dynamic load is applied, such as during an earthquake. A lower shore connection stiffness corresponds to a lower magnitude of the load transmitted to the bored tunnel. Even when no dynamic load is applied, the earth pressure owing to the weight of the surrounding soil acts on the bored tunnel. The loads acting on the crown and sidewall of the bored tunnel were observed to evaluate the effect of the load transmitted from the SFT in greater detail (Fig. 13). Consequently, the magnitude of the force applied to the crown section of the bored tunnel did not differ significantly from the magnitude of the earth pressure. This result indicates that the shear stress increase due to lateral motion is not significant. However, the magnitude of the force acting on the sidewall increased by a large amount as the stiffness of the joint increased.

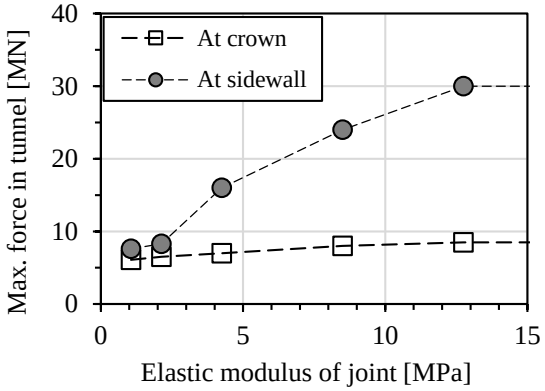

Fig. 13 Maximum forces applied at the crown and sidewall of the bored tunnel with various shore connection stiffness values

Therefore, to consider the stability of the bored tunnel, it is necessary to understand the behaviors of the tunnel and ground under a specific condition. Additionally, it is important to determine the region that is most at risk of failure according to the direction of the applied load and to determine the appropriate stiffness of the joint of the shore connection.

4.2.4 Ground surrounding the shore connection

The ground surrounding the shore connection experienced continuous deformation according to the dynamic behavior of the SFT. Because the ground model was constructed using an elastoplastic model, the plastic strain that occurred during the dynamic behavior must be considered. When the concrete joint was installed as the shore connection, the stress transferred to the ground was significant, causing considerable strain, as shown in Fig. 14(a). Using the flexible joint, the strain in the ground significantly decreased, as shown in Fig. 14(b). Observing the shear and normal stresses at the interface between ground and bored tunnel, the stresses increased as stiffer joints were used for the shore connection. Contrary to the results obtained for the bored tunnel, the increase in shear stress according to the increase in the joint stiffness was greater than that of the normal stress (Fig. 15). When a softer joint was used, the shear stress was smaller than the normal stress. These results are similar to those observed in the bored tunnel. It is expected that the strain in the normal direction increases according to a repeated dynamic load; as a result, the maximum normal stress is smaller than the maximum shear stress.

5. Discussion

5.1 Effects of the ring joint according to the boundary condition

As a result of analyzing the effects of the fixed and ground boundaries, it was confirmed that the boundary effect can vary depending on the magnitude of the dynamic load applied to the SFT and that a stiff ground boundary

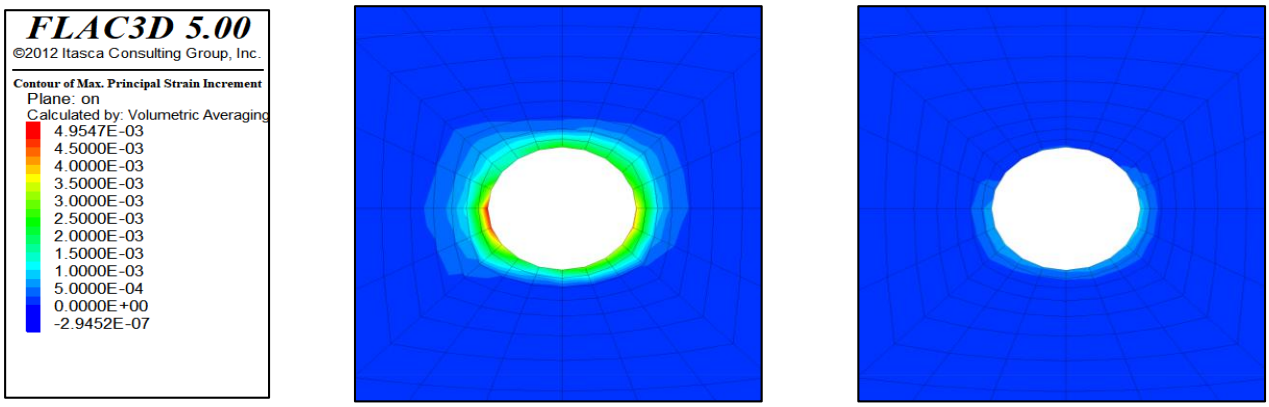

(a) (b)

Fig. 14 Principal strain distributions in the ground surrounding the shore connection with a joint composed of (a) concrete and (b) rubber under dynamic loading conditions

accompanying a small magnitude of ground strain yields similar results to a fixed boundary. Because the ring joint is attached to the boundary, its effect changes depending on the boundary conditions. The effects of the joint stiffness in this study were observed under the stiff boundary condition, and the effect of the ring joint may be insignificant in the soft boundary condition. If the stiffness of the material constituting the boundary is very large compared with the stiffness of the ring joint (e.g., rock-type ground), the effect of joint stiffness will dominate this relationship. However, if the boundary material stiffness is low compared to the ring joint stiffness (e.g., clay-type ground), the ground at the boundary deforms more than the joint, and it is expected to exhibit a greater influence on the dynamic SFT behavior. Therefore, to examine the characteristics of the shore connection behavior more precisely, an effect analysis according to the ratio of the ground and joint stiffnesses is required.

5.2 Shore design for the dynamic stability of an SFT

As the joint stiffness was decreased, the magnitude of SFT oscillation increased, its frequency decreased, and the magnitude of the stress applied to the ground connection decreased. The effects of such a low-stiffness joint have conflicting results in terms of the dynamic stability of shore connections with reduced stress at the shore connection and increased displacement of the SFT. In particular, considering that a general wave load is in the low-frequency range, a low-stiffness joint can cause an increase in the oscillation magnitude of the SFT and a decrease in the resonance frequency, which increases the risk of resonance in a marine environment. Therefore, when determining the joint stiffness in the shore-connection design of an SFT, the stability of the SFT such that it prevents resonance by avoiding the predominant loading frequency (Karabork *et al.* 2014) should be carefully considered. The joint stiffness should be low to reduce the forces acting on the ground and tunnel members at the shore connection; however, at the same time, appropriate joint stiffness should be derived considering the stability of this system to avoid SFT resonance in low-loading-frequency conditions.

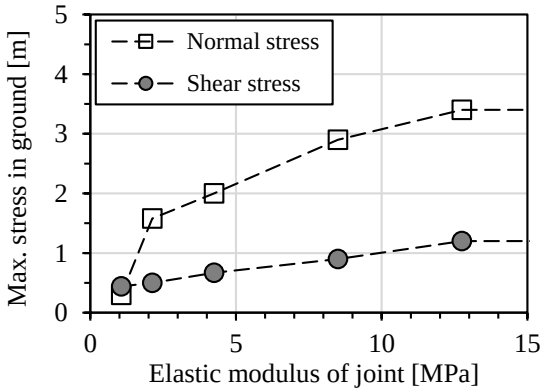

Fig. 15 Normal and shear stresses in the ground surrounding the shore connection with various shore connection stiffness values

Analysis of the results of the normal and shear stresses (Fig. 15) acting at the interface between the bored tunnel and surrounding ground at the shore connection and the loads applied on the crown and sidewall of the bored tunnel (Fig. 13) confirmed that the risk of side wall failure in the tunnel was high when a lateral load was applied to the SFT. SFTs are generally designed to obtain a buoyant force greater than their own weight and are stable against vertical motion because they receive a vertical downward force from the mooring line to maintain their depth (Long *et al.* 2015). The lateral motion of an SFT can also be restricted by adjusting the angle of the mooring line, but the magnitude of the lateral behavior has been observed to be larger than that of the vertical behavior (Chen *et al.* 2020). Therefore, when examining the stability of the ground connection according to the dynamic SFT behavior, the stability of the side wall of the bored tunnel should be carefully considered.

5.3 Consideration of ground nonlinearity

In this study, ground nonlinearity was considered using the hysteretic model proposed by Hardin and Drnevich (1972), and the ground properties were degraded according to ground deformation. However, under the load magnitude

and ground stiffness conditions investigated in this study, the strain of the ground was very small (less than 0.01%); therefore, the nonlinearity of the ground was not significant. However, if the dynamic load becomes larger or a ground boundary with low stiffness is considered, significant ground deformation occurs according to the dynamic SFT behavior, and therefore, the modulus degradation of the ground may be significant. In addition, as a dynamic load is repeatedly applied, the modulus degradation and strain continue to intensify and negatively affect the dynamic stability (Liang *et al.* 2020). Additionally, the modulus degradation of the ground can cause an increase in the magnitude of the SFT oscillation and a decrease in the resonance frequency, thereby increasing the resonance risk. Therefore, it is necessary to analyze the nonlinear behavior of the ground when a large strain is expected at the shore connection.

6. Conclusions

In this study, an SFT and its shore connection point were simulated using a numerical method, and the behavioral characteristics according to the shore design, including the boundary condition and joint stiffness, were analyzed under static and dynamic conditions.

The effect of the boundary condition was evaluated by simulating both the fixed and ground boundaries at the shore connection of the SFT. The ground simulated in this study was assumed to be homogenous granite; therefore, only a small strain occurred under the given load conditions. For this reason, there was no significant difference between the two boundary conditions, but a larger SFT displacement and a smaller stress in the shore connection were observed in the case of the ground boundary, where a slight deformation occurred compared to that of the fixed boundary condition. The small deformation at the ground boundary also contributed to the occurrence of low ground nonlinearity. Therefore, it is necessary to study the influence of the nonlinearity of the ground on the dynamic SFT behavior considering soft ground conditions in future studies.

The ring-shaped joint connecting the SFT and bored tunnel in the shore connection exhibited a much greater effect than the boundary condition on the dynamic SFT characteristics. The static analysis results showed a similar tendency to previous findings and showed that the use of a low-stiffness joint could improve the stability at the shore connection by relieving the stress concentration. However, when considering the behaviors of the SFT and shore connection under dynamic load conditions, it was confirmed that the use of a flexible joint has the potential to cause excessive displacement amplification. It was confirmed that the dynamic load transferred to the bored tunnel decreased as the stiffness of the joint between the SFT and bored tunnel decreased. As a result of observing the strain and stress distributed in the ground surrounding the shore connection, the use of a soft joint caused a decrease in the stress and strain at the shore connection. Considering the overall results, when an SFT was connected to the shore through a joint with a low stiffness, the deformation of the shore connection increased and the magnitude of the stress acting on the surrounding tunnels and ground decreased. However, the use of a soft joint also caused the SFT to be vulnerable to resonance because it lowers the resonance frequency of the SFT.

Therefore, it can be concluded that decreasing the stress concentration at the shore connection point and preventing resonance should be utilized when designing SFTs considering their dynamic stability. Because a low joint stiffness corresponds to the relief of the stress concentration and a high joint stiffness may be used to reduce the risk of resonance, it is necessary to determine the optimal joint stiffness that can satisfy both design considerations simultaneously. The optimal stiffness may be derived by performing parametric studies on the joint stiffness under specific SFT construction environment conditions, wherein the magnitude and frequency of the dynamic load may be investigated. Although this study considered only one environmental condition, the numerical results and approaches used for shore connection design proposed in this study can contribute to future research related to detailed SFT design.

Acknowledgments

The research described in this paper was financially supported by a National Research Foundation of Korea (NRF) grant funded by the Korean government (MSIT) (No. 2017R1A5A1014883).

References

Chen, X., Chen, Z., Cai, S., Xu, W., Zhuo, X., Lv, J. and Zhao, J. (2020), "Numerical investigation of dynamic responses and mooring forces of submerged floating tunnel driven by surface waves", *Sci. Rep*. **10**(1), 1-19. https://doi.org/10.1038/s41598-020-75907-8.

Cifuentes, C., Kim, S., Kim, M. and Park, W. (2015), "Numerical simulation of the coupled dynamic response of a submerged floating tunnel with mooring lines in regular waves", *Ocean Syst. Eng.*, **5**(2), 109-123. https://doi.org/10.12989/ose.2015.5.2.109.

Grant, A. (1986), "A submerged floating tunnel solution to a crossing for the Strait of Messina", *Symposium on Strait Crossings*, **353**, 365.

Hardin, B.O. and Drnevich, V.P. (1972), "Shear modulus and damping in soils: design equations and curves", *J. Soil Mech. Found. Div.*, **98**(7), 667-692. https://doi.org/10.1061/jsfeaq.0001760.

Itasca, F.D. (2013), *Fast lagrangian analysis of continua in 3 dimensions*.

Jakobsen, B. (2010), "Design of the submerged floating tunnel operating under various conditions", *Procedia Eng.*, **4** 71-79. https://doi.org/10.1016/j.proeng.2010.08.009.

Jiang, B., Liang, B. and Wu, S. (2018), "Feasibility study on the submerged floating tunnel in Qiongzhou strait, China", *Pol. Marit. Res*., https://doi.org/10.2478/pomr-2018-0066.

Jin, C. and Kim, M. (2017), "Dynamic and structural responses of a submerged floating tunnel under extreme wave conditions", *Ocean Syst. Eng.*, **7**(4), 413-433.

https://doi.org/10.12989/ose.2017.7.4.413.
Jin, C. and Kim, M. (2021), "The effect of key design parameters on the global performance of submerged floating tunnel under target wave and earthquake excitations", *Comput. Model. Eng. Sci*., **128**(1), 315-337. https://doi.org/10.32604/cmes.2021.016494.
Jin, R., Gou, Y., Geng, B., Zhang, H. and Liu, Y. (2020), "Coupled dynamic analysis for wave action on a tension leg-type submerged floating tunnel in time domain", *Ocean Eng*., **212**, 107600. https://doi.org/10.1016/j.oceaneng.2020.107600.
Kang, S.J., Kim, J.T. and Cho, G.C. (2020), "Preliminary study on the ground behavior at shore connection of submerged floating tunnel using numerical analysis", *Geomech. Eng.*, **21**(2), 133-142. https://doi.org/10.12989/gae.2020.21.2.133.
Karabork, T., Deneme, I.O. and Bilgehan, R.P. (2014), "A comparison of the effect of SSI on base isolation systems and fixed-base structures for soft soil", *Geomech. Eng.*, **7**(1), 87-103. https://doi.org/ 10.12989/gae.2014.7.1.087.
Kuhlemeyer, R.L. and Lysmer, J. (1973), "Finite element method accuracy for wave propagation problems", *J. Soil Mech. Found. Div*., **99**(5), 421-427. https://doi.org/10.1061/JSFEAQ.0001885.
Liang, P., Gao, Y., Zhou, Y., Zhu, C. and Sun, Y. (2020), "Solution for surrounding rock of strain-softening considering confining pressure-dependent Young's modulus and nonlinear dilatancy", *Geomech. Eng.*, **22**(4), 277-290. https://doi.org/10.12989/gae.2020.22.4.277.
Long, X., Ge, F. and Hong, Y. (2015), "Feasibility study on buoyancy–weight ratios of a submerged floating tunnel prototype subjected to hydrodynamic loads", *Acta Mech. Sin*., **31**(5), 750-761. https://doi.org/10.1007/s10409-009-0233-y.
Long, X., Ge, F., Wang, L. and Hong, Y. (2009), "Effects of fundamental structure parameters on dynamic responses of submerged floating tunnel under hydrodynamic loads", *Acta Mech. Sin.*, **25**(3), 335-344. https://doi.org/10.1007/s10409-009-0233-y.
Martinelli, L., Barbella, G. and Feriani, A. (2010), "Modeling of Qiandao Lake submerged floating tunnel subject to multi-support seismic input", *Procedia Eng*., **4**, 311-318.
Martire, G. (2010), *The development of Submerged Floating Tunnels as an innovative solution for waterway crossings*, Università degli Studi di Napoli Federico II, Italy.
Mazzolani, F., Faggiano, B. and Martire, G. (2010), "Design aspects of the AB prototype in the Qiandao lake", *Procedia Eng.*, **4**, 21-33. https://doi.org/10.1016/j.proeng.2010.08.005.
Mazzolani, F.M., Landolfo, R., Faggiano, B. and Esposto, M. (2007), "A submerged floating tunnel (Archimedes bridge) prototype in the Qiandao lake (PR of China): research development and basic design", *Costr. Met.*, **5**, 45-63.
NPRA (2016), *Bjørnafjord Submerged Floating Tube Bridge: K3/K4 Technical Report*.
Park, J., Kang, S.J., Hwang, H.J. and Cho, G.C. (2022), "Numerical study on the resonance behavior of submerged floating tunnels with elastic joint", *Geomech. Eng*., **29**(3), 207-218. https://doi.org/10.12989/gae.2022.29.3.207.
Seed, H.B., Wong, R.T., Idriss, I. and Tokimatsu, K. (1986), "Moduli and damping factors for dynamic analyses of cohesionless soils, *J. Geotech. Eng*., **112**(11), 1016-1032. https://doi.org/10.1061/(asce)0733-9410(1986)112:11(1016).
Won, D. and Kim, S. (2018), "Feasibility study of submerged floating tunnels moored by an inclined tendon system", *Int. J. Steel Struct*., **18**(4), 1191-1199. https://doi.org/10.1007/s13296-018-0102-2.
Xiao, J. and Huang, G. (2010), "Transverse earthquake response and design analysis of submerged floating tunnels with various shore connections", *Procedia Eng*., **4**, 233-242. https://doi.org/10.1016/j.proeng.2010.08.027.
Youshi, H. and Fei, G. (2010), "Dynamic response and structural integrity of submerged floating tunnel due to hydrodynamic load and accidental load", *Procedia Eng.*, **4**, 35-50. https://doi.org/10.1016/j.proeng.2010.08.006.